DESIGN AND IMPLEMENTATION OF THE POWERED SELF-CONTAINED AMPRO PROSTHESES

A Thesis

by

JONATHAN CORWIN HORN

Submitted to the Office of Graduate and Professional Studies of
Texas A&M University
in partial fulfillment of the requirements for the degree of

MASTER OF SCIENCE

Chair of Committee,	Aaron Ames
Committee Members,	Bryan Rasmussen
	Srinivas Vadali
Head of Department,	Andreas Polycarpou

August 2015

Major Subject: Mechanical Engineering

Copyright 2015 Jonathan Corwin Horn

ABSTRACT

This thesis presents a complete methodology for translating robotic walking to powered prostheses, and demonstrates this framework on two novel custom built powered prostheses, AMPRO. Motivated by methods that have successfully generated dynamically stable walking gaits on bipedal robots, reference human locomotion data is collected via Inertial Measurement Units (IMU) and stable walking gaits are generated using the framework of human-inspired optimization and control. Next two novel transfemoral protheses are designed and custom built based on the understanding obtained from the collection of human data and gait generation. For experimental realization, the IMUs are mounted on the healthy human leg to estimate human intention during walking on-line, and serves as the feedback interaction point between human and prosthesis. The end result is the experimental verification of the proposed methodology in achieving stable and robust locomotion on a powered prosthesis. Furthermore it is concluded that reducing the weight of AMPRO I, through the design of AMPRO II, improves the performance of the prosthesis and comfort of the human subject.

DEDICATION

To my mother, for always believing in me.

ACKNOWLEDGEMENTS

I would like to thank my family for always being supportive during my time as a student. I would not have made it this far with out them. I would like to thank my parents for encouraging me to heart in everything I have done. My accomplishments are layered with their love and support.

I would attribute my work ethic and mindset to my advisor, Dr. Ames. His positive outlook and ”keep pushing” mentality have continually lead me in the right direction. I would also like to thank my friends and teammates on the AMPRO team, Huihua, Victor and Jake for being a part of the best team of friends I have ever worked with. Without the AMPRO team I am sure this work would not have been possible.

TABLE OF CONTENTS

Page

LIST OF FIGURES

FIGURE Page

LIST OF TABLES

TABLE Page

1. INTRODUCTION

According to the National Center for Health Statistics approximately 222,000 people in the United States are transfemoral amputees [14], and technological innovations have yet to benefit the lives of those living with limb loss. The current market for transfemoral prostheses is dominated by passive prosthetic devices. As a result of this rudimentary approach, the day-to-day life of amputees adjusting after surgery is anything but simple. Transfemoral limb loss poses many challenges for an amputee such as increased energy requirements and stability issues [39]. One way to combat these issues and restore natural locomotion is through the use of a powered prosthesis. That is, a device that supplies significant net positive power output at both the ankle and knee joints. This type of device would demand challenging requirements be fulfilled: 1) A self-contained power generation infrastructure that supplies power on par with or better than that of a normal limb; 2) A controller design that gathers the user's intention and provides natural interaction between the user and the prosthesis.

Figure 1.1: Current day commercially available prostheses Otto Bock C-Leg (left) and iWalk BiOM (right). [1]

1.1 Literature Review

Prior work involving powered knee or powered ankle transfemoral prostheses is a well documented area of interest. Most notably, Flowers et al. [16], [17] developed a hydraulically actuated powered knee prosthesis. This tethered device led to the formulation of a gait control scheme where the modified trajectory of a healthy leg is mirrored on the opposing side, known as "echo control" [15]. In addition to knee joint specific prostheses, other groups have successfully developed the use active ankle joint prostheses. Klute presented a device in [22] that utilized pneumatic McKibben actuators for an active ankle joint, yet did not describe walking gait control algorithms. More recently Herr et al. [19, 13] developed a ballscrew actuated ankle-foot prosthesis. Herr was able to verify such a device does improve an amputee gait when compared to standard passive prostheses. New developments of an active knee and ankle prosthesis have recently been documented as well [11]. Similarly, [41] have developed the design of a tethered powered ankle and knee prosthesis that used double acting pneumatic actuators to achieve level ground walking.

1.2 Objective and Contribution

Rather than accepting previous strategies as the standard, knowledge of the human body is leveraged to develop a new novel prosthesis with a human-inspired control scheme [30]. The human body (which uses 57 muscles for walking locomotion [32]) is a very complex system that can not be precisely modeled with current technology. However, this thesis will construct a low-level representation of the human system. From a control stand point, the human body will be viewed as a "black box" where particular outputs of the system can be represented by time-based functions [18]. With these outputs, feedback linearization control can then be used to achieve stable flatground walking [43]. This control approach is similar to other approaches used by researchers in biomechanics. Specifically, [42] and [44] were able to achieve stable walking for a 5-link robot using a combination

of human data and hybrid zero dynamics. However unlike works previous, this research will apply this control strategy to design, construct and develop a novel prosthesis prototype, AMPRO. AMPRO is an actively powered, transfemoral, prosthesis that has been developed by the author.

In this thesis, a new prosthesis prototype is designed based off of anthropomorphic performance and structure. Then a human-inspired controller is utilized to develop the prosthesis and achieve stable human-like flat ground walking. The study begins an examination of the human system during locomotion with a particular focus on the lower body performance and structure. Next, this knowledge is then used to design and develop AMPRO. Development of the device included mechanical design of the device, actuator selection and assembly, sensor package, and a control strategy. The control of the device was translated from robotic applications to powered prostheses with the intent of increasing positive human interaction with the device. Testing of the device was performed with an able bodied test subject with an able-bodied adapter for initial debugging. The final tests were performed with a single unilateral transfemoral amputee test subject demonstrating the device in a laboratory setting as well as real world application.

1.3 Thesis Structure

The structure of this Thesis begins with the study of human locomotion experiments in Chapter 2. Chapter 3 will discuss the bipedal robotic model that will be used to model the prosthetic device. Then the design of the active powered knee and ankle joint prosthesis (AMPRO) is outlined in Chapter 4. Chapter 5 presents the preliminary test results for flat ground walking with an able bodied test subject. Design considerations are then discussed at the end of the chapter.

2. HUMAN LOCOMOTION

The most genuine source of information on human locomotion during walking is found at the human body. This section provides a summary of the analysis of human walking. In an effort to reduce monetary cost, human walking data was collected from Inertial Measurement Units (IMUs) for flat ground walking. A single step from the experiment is isolated and an *canonical walking function* is used to represent the kinematic output of the human body for flat ground walking.

2.1 Human Canonical Walking Function

In an effort to achieve human-like robotic walking, we turn to the most prevalent source for inspiration, the human body. In particular, a low-cost inertial motion capture system with IMUs is developed and interfaced with the human-inspired control approach. This system is first used to capture the walking trajectories of a human subject, and is then fitted to a canonical function. The Human Canonical Walking Function will be reviewed, and the fitted average walking data for a particular test subject will be presented.

Previous work [36] has shown that during level ground walking, particular kinematic outputs can be represented by a single universal function. This function is termed the canonical human function (CHF), and was shown to have a solution similar to that of a linear spring-damper system under constant force. Different from previous work, this work will use this function practically for operation of a prosthetic device. Specifically, the solution of a linear spring-mass-damper system is given as:

$$y_{cwf}(t) = e^{-\zeta\omega_n t}(c_1 cos(\omega_d t) + c_2 sin(\omega_d t)) + \frac{g}{\omega_n^2}. \tag{2.1}$$

where c_1 and c_2 are constants that are solved for using the initial position and velocity of

the system $(y(0), \dot{y}(0))$; the damping ratio and natural frequency are defined as ζ and ω_n respectively; the damped natural frequency is ω_d and g is the constant gravity term.

Eq. 2.1 can be reformulated into a simpler representation, which will be termed the Canonical Walking Function (CWF) as:

$$y_{cwf}(t, \alpha) = e^{-\alpha_4 t}(\alpha_1 cos(\alpha_2 t) + \alpha_3 sin(\alpha_2 t)) + \alpha_5. \tag{2.2}$$

which is characterized by the parameter set $\alpha = [\alpha_1, \alpha_2, \alpha_3, \alpha_4, \alpha_5]$. Comparing the simplified form with the original solution of the linear spring-mass-damper shows that:

$$\alpha = \begin{bmatrix} \alpha_1 \\ \alpha_2 \\ \alpha_3 \\ \alpha_4 \\ \alpha_5 \end{bmatrix} = \begin{bmatrix} \zeta\omega_n \\ c_1 \\ \omega_d \\ c_2 \\ g/\omega_n^2 \end{bmatrix}, \tag{2.3}$$

Rather than trying to piece together the complex human system used for walking, a control theorist perspective will be used. If the human walking system is viewed as a "black box," the problem can be reformulated to find what outputs of the black box will characterize the behavior of the system. Similar approaches that use a different fitting techniques have been used in the robotics community. Specifically, polynomial functions were used in [23] and B-spline fitting techniques were used in [46]. Also a Bezier series has been applied in [42] and [44]. However, in order to reduce the complexity, the CWF is utilized here because of its simpler form that needs less parameters to characterize human walking behavior. Now the method used to obtain joint angles for an individual test subject will now be explained

2.2 Motion Capture with IMU

There have been many methods proposed for ambulatory measurement of human joint angles. In particular, Luinge and Veltink [25] proposed a Kalman filter which integrates the 3D angular velocity while applying heading corrections based on accelerometer readings. This approach is prone to integration drift of the gyroscope for systems which need to operate for long durations of time such as prostheses. A more advanced kinematic filtering method was proposed by Roetenberg et al. [31] for the XSens MVN motion capture suit. This approach uses a kinematic model of the individual body segments which is used to update a Kalman filter and provide the positions of each joint and segment of the body. Motion capture systems have also been shown to be effective for robotic teleoperation such as the method proposed by Miller et al. [27] in which an inertial motion capture system was successfully used to teleoperate the NASA Robonaut This system used a complementary filter to fuse accelerometers, gyroscopes, and magnetometers to estimate poses which were then used to compute an inverse kinematic relationship for pose recreation on the robot.

The algorithm used for motion capture in this work is a modification of the model-based EKF first presented by Šlajpah et al. [38]. In this approach, the human extremeties are modelled as a kinematic chain built from a location of negligible acceleration. The algorithm used in this work is different in two aspects: the kinematic model of the human legs is assumed to be composed of joints with ranges of motion limited to flexion/extension, and the kinematic chain is built from the hip. Since AMPRO has restricted actuation in solely the saggital plane and because joint variations in the coronal plane are not used in the proposed control approach, only measurements resulting in joint flexion and extention are used in the model update. Additionally, we assume that the forward velocity of the hip is constant and that sinusoidal movement of the hip in the vertical direction will yield negligible acceleration in comparison to walking dynamics.

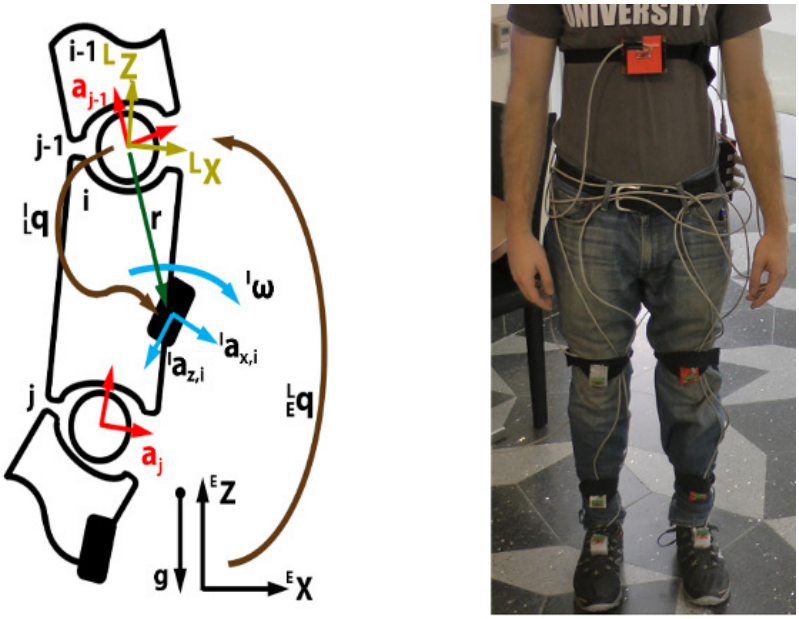

Figure 2.1: IMU kinematic chain (left) and sensor setup (right) [45]

An EKF is instantiated for each segment in the model and updated sequentially along the kinematic chain from the hip. Each update uses the known acceleration from the proximal joint along with measured segment angular velocity and linear acceleration to determine the global orientation of the segment and the acceleration of the distal joint, which is passed to the next EKF in the chain. The estimated state of each segment $\hat{x}_k^+$ is updated during the integration step:

$$\hat{x}_k^+ = \hat{x}_k^- + \mathbf{K}_k(z_k - h(\hat{x}_k^-)), \tag{2.4}$$

in which the Kalman gain $\mathbf{K}_k$ is computed based on the error covariance and the stochastic parameters assigned to the states and measurements, $\hat{x}_k^-$ is the estimated state before the Kalman update, z_k is the current sensor measurement, and $h(\hat{x}_k^-)$ is the predicted measurement values based on the previous state estimate. Each EKF provides its quaternion

attitude in the global frame, from which the joint rotation q_j can be found as:

$$q_j = q_P^* \otimes q_D, \tag{2.5}$$

where q_P^* denotes the quaternion conjugate, $\otimes$ is the quaternion product, q_D is the distal segment orientation and q_P is the proximal segment orientation.

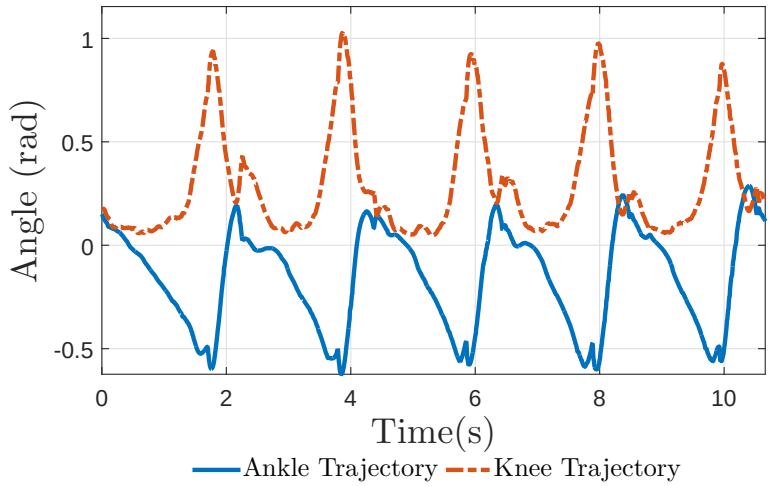

Figure 2.2: IMU data capture for five steps.

2.3 Locomotion Experiments

An obvious problem encountered when capturing a gait for an amputee is the lack of original locomotion data for the amputee. One possible approach involves capturing the trajectories from an amputee with wearing a passive prosthesis. However this technique has the potential to generate an asymmetric gait. On the other side of the spectrum, human gait researchers and biomechanists have found that humans share a common pattern of joint trajectories during locomotion [45]. Therefore, a different and feasible approach is

to use the nominal trajectories obtained from healthy subjects as the initial test gait for the amputee.

During the experiment, the subject was asked to walk along a straight line for several steps while wearing seven IMUs to capture the walking behavior of the feet, shanks, thighs, and torso. The joint states are estimated and collected with the EKF algorithm. Then the joint angles are calculated by converting the joint rotation found in (2.5) to an Euler angle representation. Finally, several steps are averaged to yield their unique trajectories for optimization. To verify that the EKF method is successfully capturing the human motion, knee and ankle joint angles of a healthy subject are compared to a standard set of saggital plane gait kinematics findings by Winter [45] as shown in Fig. 2.3.

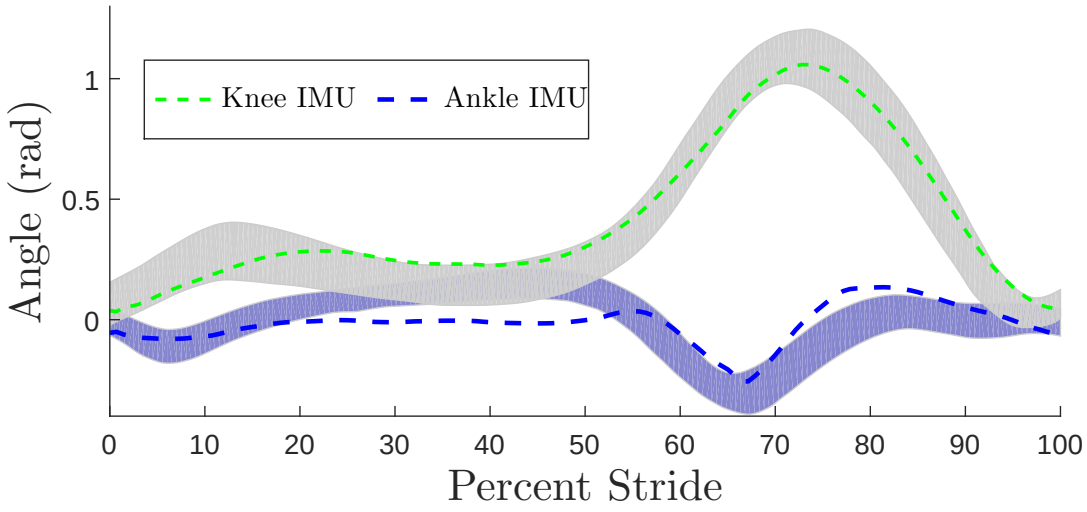

Figure 2.3: IMU data capture compared to data recorded by Winter [45]

The IMUs used for data collection are Invensense MPU-9150 IMUs that consist of a tri-axial gyroscope (with a range of $\pm 500^{\circ}/s$) and a tri-axial accelerometer (that has a range of $\pm 4g$).

For data collection, a healthy human subject of similar anthropomorphic dimensions as the amputee was used to capture a flat ground walking gait. The collection of the trajectories was accopmlished using seven IMUs attached to the user, providing joint angle measurements for all joints of the legs and torso. The subject was asked to walk for several steps which were then averaged to yield unique trajectories. In an effort to reduce ”noisy” data collection, a model based Extended Kalman Filter (EKF) was used to obtain accurate join angle information in the same way as [38].

3. PROSTHESIS GAIT DESIGN

In this section, a bipedal roboot will be utilized to model the human-prosthesis system. Additionally, the technique of human inspired optimization will be review and used to modify the captured human trajectories, similar to [10]. The end result will be a stable flat-footed walking gait that will be implemented using PD control.

3.1 Bipedal Robot Model

In this work, The human-prosthesis system will be modeled as a 7-link bipedal robot (consisting of one torso and two thighs, calves and feet) with dimensions similar to those of the test subject. Since the system will exhibit both continuous and discrete dynamics during operation, the bipedal robot will be represented as a hybrid system with theconfiguration space Q_R with coordinates given by: $\theta = (\theta_{sa}, \theta_{sk}, \theta_{sh}, \theta_{nsh}, \theta_{nsk}, \theta_{nsa})^T$ as shown in Fig. 3.2.

This work will use the same approach as described here, [37], to model the system. For a 6-DOF robot, six mutually exclusive kinematic outputs are required to unambiguously characterize motion of the system. From the collected human data, the six following outputs seem to accurately describe the motion of the system:

1. The linearized hip velocity p_{hip}

$$\delta p_{hip} = -(L_c + L_t)\theta_{sa} - L_t\theta_{sk}$$

2. The linearization of the slope of the non-stance leg m_{nsl}

$$\delta m_{nsl} = -\theta_{sa} - \theta_{sk} - \theta_{sh} + \theta_{nsh} + \frac{L_c}{L_c+L_t}\theta_{sk}$$

3. The angle between the non-stance foot and the ground θ_{nsf}

$$\theta_{nsf} = \theta_{sa} + \theta_{sk} + \theta_{sh} - \theta_{nsh} - \theta_{nsk} - \theta_{nsa}$$

4. The torso angle θ_{tor}

$$\theta_{tor} = \theta_{sa} + \theta_{sk} + \theta_{sh}$$

5. The stance knee angle θ_{sk}

6. The non-stance knee angle θ_{nsk}

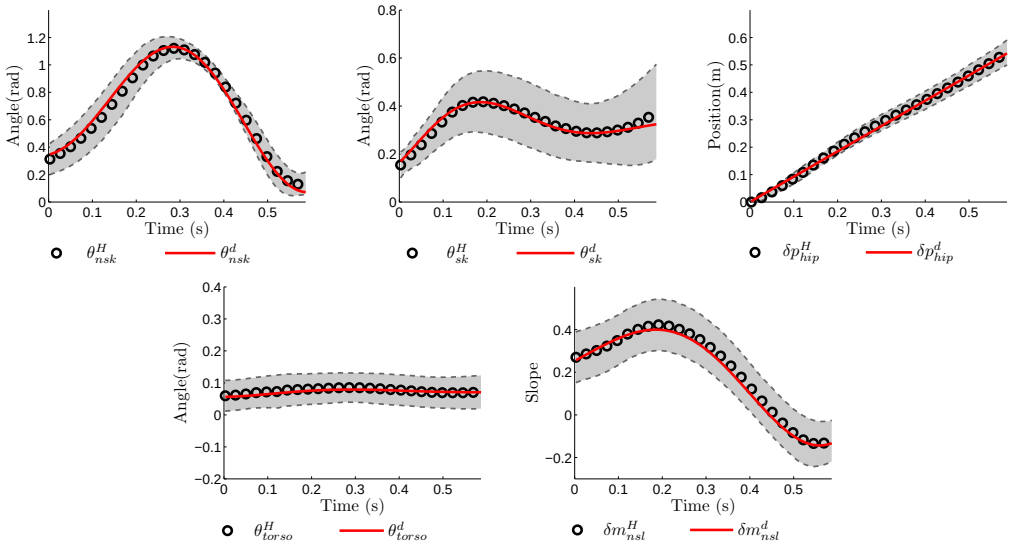

Figure 3.1: Selected human outputs fitted against the nominal human values

With these six outputs, the average outputs are calculated from the collected human data. Then using the model of the bipedal system, the Lagrangian can be formed as:

$$L(\theta, \dot{\theta}) = \frac{1}{2}\dot{\theta}^T D(\theta)\dot{\theta} - V(\theta) \tag{3.1}$$

The equations of motion of the continuous dynamics are found using the Euler-Lagrange formula as:

$$D(\theta)\ddot{\theta} + H(\theta, \dot{\theta}) = Bu, \tag{3.2}$$

where in this case, $D(\theta) \in \mathbb{R}^{6\times 6}$ is the inertial matrix and $H(\theta, \dot{\theta}) \in \mathbb{R}^{6\times 1}$ contains the

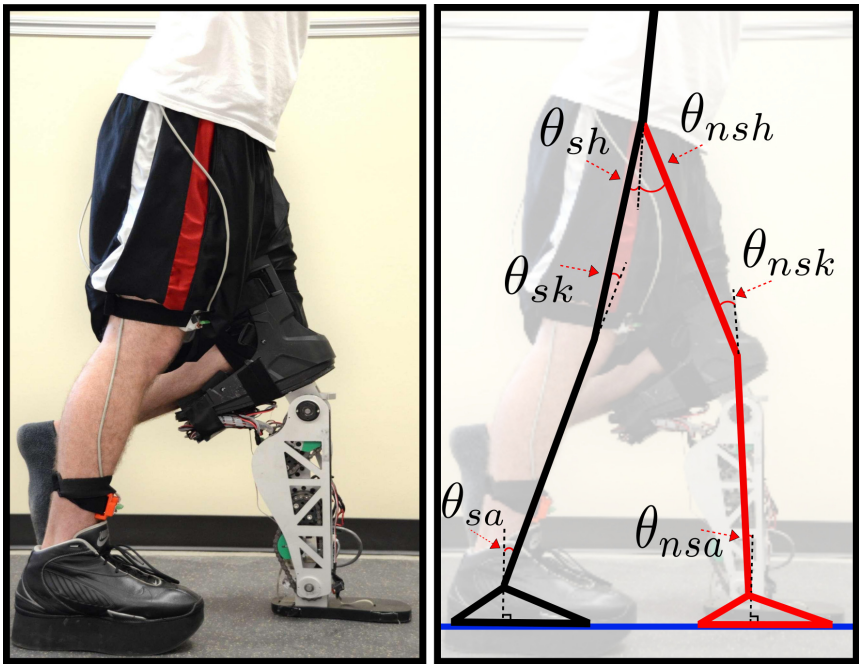

Figure 3.2: Configuration space of the human-robot system.

terms resulting from the Coriolis effect $C(\theta, \dot{\theta})\dot{\theta}$ and the gravity vector $G(\theta)$ [33]. The torque map $B = I_6$ and u, is the vector of torque inputs. Now defining $x = (\theta; \dot{\theta})$, the affine control system $\dot{x} = f(x) + g(x)u$ is obtained by rearranging (3.2) [33]. Additionally, a perfectly plastic impact assumption is used to model the discrete behavior that will be exhibited by the system; more details can be found in [6, 21].

3.1.1 Human-Inspired Outputs

With the goal of characterizing human walking, treating the very complex human system as a "black box" will be used [37]. The goal becomes to drive the actual robot outputs $y^a(\theta)$ to the desired human outputs $y^d(t,\alpha)$ that are found [35]. These outputs can be represented by the *canonical walking function* (CWF) with a parameter set α in the formula as:

$$y_{cwf}(t,\alpha) = e^{-\alpha_4 t}(\alpha_1 cos(\alpha_2 t) + \alpha_3 sin(\alpha_2 t)) + \alpha_5. \tag{3.3}$$

This function is shown to be able to characterize human motion primitives universally including walking, running and stair climbing in previous work [6, 49]. For the bipedal robotic model considered here, a total of 6 outputs are of interest. These outputs include the forward hip velocity (*hip*), knee angles (*sk*, *nsk*), non-stance slope (*nsl*), torso angle (tor) and non-stance foot angle (nsf); for details, refer to [48]. We then introduce the human-inspired outputs:

$$y(\theta,\dot{\theta},\alpha) = \begin{bmatrix} y_1(\theta,\dot{\theta},\alpha) \\ y_2(\theta,\alpha) \end{bmatrix} = \begin{bmatrix} y_1^a(\theta,\dot{\theta}) - v_{hip} \\ y_2^a(\theta) - y_2^d(\rho(\theta),\alpha) \end{bmatrix}, \tag{3.4}$$

where $y_1(\theta,\dot{\theta}) = y_1^a(\theta,\dot{\theta}) - v_{hip}$ is the difference between the actual and desired hip velocity, and relative degree two outputs $y_2(\theta,\alpha) = y_2^a(\theta) - y_2^d(\rho(\theta),\alpha)$ contain the differences between the actual and desired relative degree two outputs. Note that, the desired relative degree two outputs are defined as $y_2^d(\rho(\theta),\alpha) = [y_{cwf}(\rho(\theta),\alpha_i)]_{i\in O}$ with $\alpha_i = (\alpha_{i,1},\alpha_{i,2},\alpha_{i,3},\alpha_{i,4},\alpha_{i,5})$ in (2.2), and $O = \{sk, nsk, nsl, tor, nsf\}$ is the set of relative degree two outputs. The parameters of all of the outputs are then combined to yield a single vector $\alpha = (v_{hip},\alpha_{sk},\alpha_{nsk},\alpha_{nsl},\alpha_{tor},\alpha_{nsf}) \in \mathbb{R}^{26}$.

After observing and studying human locomotion the position of the hip, $\delta p_{hip}(\theta)$, was found to linearly increase as a function of time. This motivate the construction of the phasing variable:

$$\rho(\theta) = (\delta p_{hip}(\theta) - \delta p^{+}_{hip})/v_{hip}, \tag{3.5}$$

which is used to parameterize any given walking gait as indicated in the formula of the desired outputs. Note that, the initial forward position of the hip $\delta p^{+}_{hip}(\theta)$ will be decided through the optimized gait which will be discussed later.

3.2 Human-Inspired Optimization

After defining the previously stated outputs, a human-inspired controller [6] (that uses feedback linearization) can be used in such a way to drive both relative degree one and degree two outputs to zero in a stable fashion. However, the robot can be disturbed or "pushed-off" the intended trajectory when an impact is present. We therefore introduce the partial hybrid zero dynamics (PHZD) constraints [44]. These constraints will aim to yield a parameter set α that will ensure tracking of the relative degree two outputs remain invariant even when impacts occur. This will therefore guarantee stability of the walking gait during operation. In particular, the partial zero dynamics surface is defined by the following:

$$\mathbf{PZ}_{\alpha} = \{(\theta, \dot{\theta}) \in Q_R : y_2(\theta, \alpha) = \mathbf{0}, L_f y_2(\theta, \alpha) = \mathbf{0}\}, \tag{3.6}$$

and the PHZD constraints can be explicitly stated as:

$$\Delta_R(S_R \cap \mathbf{PZ}_{\alpha}) \subseteq \mathbf{PZ}_{\alpha}, \tag{PHZD}$$

where the terms Δ_R and S_R are defined as the reset map and switching surface, respectively. A more detailed explanation of these constraints can be found in [6].

By enforcing the PHZD constraints, prosthetic trajectories can be generated using a human-inspired optimization technique. This technique will generate walking gaits that are both provably stable and human-like [6, 8, 7]. More importantly, more attention must be placed on the physical limitations of the prosthesis for safety and energy conservation. One goal in particular, for example, is to optimize the torque profile to ensure the prosthesis stays within the limitations of the motor capabilities. As a result, walking gaits which require optimal torque will also decrease the energy required by the device and could potentially increase the battery life. Therefore, the optimization problem subject to the PHZD and physical constraints is stated as [9]:

$$\begin{aligned} \alpha^* = \underset{\alpha \in \mathbb{R}^{26}}{\operatorname{argmin}} \ & \mathrm{Cost}_{\mathrm{HD}}(\alpha) \\ \text{s.t} \quad & \text{PHZD Constraints}, \\ & \text{Physical Constraints}, \end{aligned} \tag{HIO}$$

where the cost function is the least-square-fit error between the collected experimental data and the CWF representation of the human outputs (3.4).

This optimization problem formed previously uses the trajectory of a healthy human test subject as the reference trajectory. This trajectory is subject to PHZD constraints (to ensure smoothness during transitions) and physical constraints (motor limitations and configuration space) such that the output walking gait can be utilized on the prosthetic device. The main advantages of using the optimization problem presented here are twofold: a) an optimal and smooth gait can be designed for a particular test subject without requiring hand tuning and, b) the output gait may be utilized directly on the prosthesis platform.

The term of stability mentioned here is specific to the mathematical stability of the designed gait, i.e., the gait has a limit cycle and is exponentially stable. While this stability property does not guarantee stable walking (w.r.t the walking balance) of the prosthetic device, it plays a key role during the nonlinear prosthetic controller development. To be more specific, the main goal of this series of work is to translate robotic walking into the design and control of the prosthesis. A mathematically stable gait is essentially important for realization of robotic walking for bipedal robots in both simulation and experiment. Utilizing this stable robotic walking, the nonlinear controller, therefore, can be verified and improved on the robots before implementing on the prosthetic device.

3.3 Prosthetic Trajectory Reconstruction

From the presented optimization problem, the parameter set α is used to define the out puts of the human. With these outputs characterizing human locomotion, we can obtain desired joint angles and angular velocities for the robot at every iteration in time. This is accomplished through the inverse projection of the Partial Hybrid Zero Dynamics surface. This is achieved using a method termed Partial Hybrid Zero Dynamics reconstruction [26]. Specifically, when the robot is on the zero dynamics surface, the coordinates are given as:

$$\xi_1 = \delta p_{hip}(\theta) := c\theta, \tag{3.7}$$

$$\xi_2 = y_1^a(\theta, \dot{\theta}) := \delta \dot{p}_{hip}(\theta) := c\dot{\theta}, \tag{3.8}$$

where c is the array defining the linearized position of the hip $\delta p_{hip}(\theta)$ [48]. As the direct result of (3.5) and (3.7), the desired relative degree two outputs can be stated as $y_2^d(\rho(\theta), \alpha) = y_2^d(\xi_1, \alpha)$. Because of the selection of linear actual relative degree two outputs, $y_2^a = H\theta$ and $\dot{y}_2^a = H\dot{\theta}$. Therefore, since the actual outputs will be equal to the desired outputs on the PHZD surface, we have the following relationships between the

desired joints states and the desired outputs of the robot given by:

$$\theta_d(\xi) = \Psi(\xi_1, \alpha) = \begin{bmatrix} c \\ H \end{bmatrix}^{-1} \begin{pmatrix} \xi_1 \\ y_2^d(\xi_1, \alpha) \end{pmatrix}, \tag{3.9}$$

$$\dot{\theta}_d(\xi) = \Phi(\xi_1, \xi_2, \alpha) = \begin{bmatrix} c \\ H \end{bmatrix}^{-1} \begin{pmatrix} v_{hip} \\ \frac{\partial y_2^d(\xi_1, \alpha)}{\partial \xi_1} \xi_2 \end{pmatrix}.$$

The result is realized by knowing ξ_1 and ξ_2 (which are the linearized position of the hip and hip velocity, respectively), the desired states can be obtained by directly using the parameter α. More importantly, the resulting joint angles and velocities are guaranteed to be smooth, human-like and optimal.

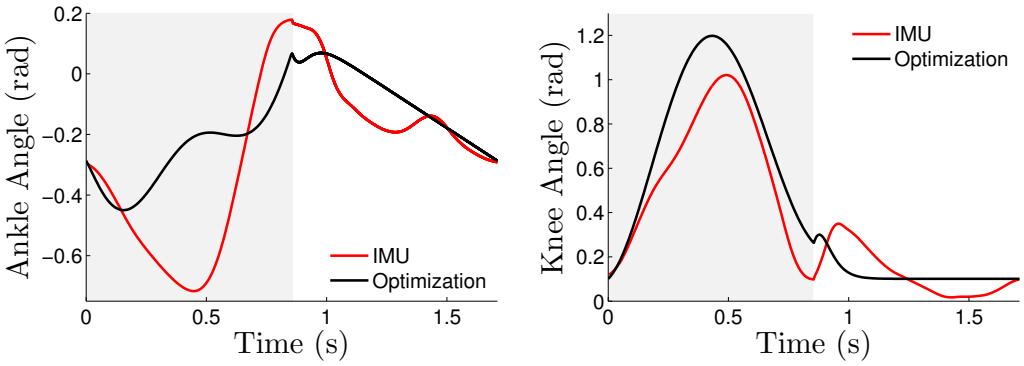

Figure 3.3: Configuration space of the human-robot system.

3.4 Control Strategy

This section will revisit human-inspired control approach. The purpose of this section is to define a control input, u, to be applied to the robotic prosthesis. Therefore, it is desired to drive the ouputs of the robot to the corresponding outputs of a human. The

control method chosen to do this is Feedback PD control, due to the complex nonlinear robotic system [33].

Specifically, a PD controller will be used to control the prosthetic device during experimentation. Based upon the methods discussed so far, the PD controller is implemented by tracking joint trajectories obtained from the PHZD reconstruction:

$$\tau_{PD} = K_P(\theta_a - \theta_d) + K_d \frac{d}{dt}(\theta_a - \theta_d) \tag{3.10}$$

where K_P and K_d are proportional and derivative constant matricies respectively. It is important to note that the values of these constants will be dependent on specific motors during implementation.

4. DESIGN OF AMPRO I

The objective of this section is to introduce the pertinent design specifications of AMPRO and explain the experiments conducted to obtain human-like locomotion. The design of AMPRO is highly influenced by how the device is used, but is also designed to maintain an aesthetically pleasing appearance.

4.1 Design Requirements

The main goal for the design of AMPRO was to produce a very powerful prosthesis with the ability to perform operation modes of an average humans day-to-day life.

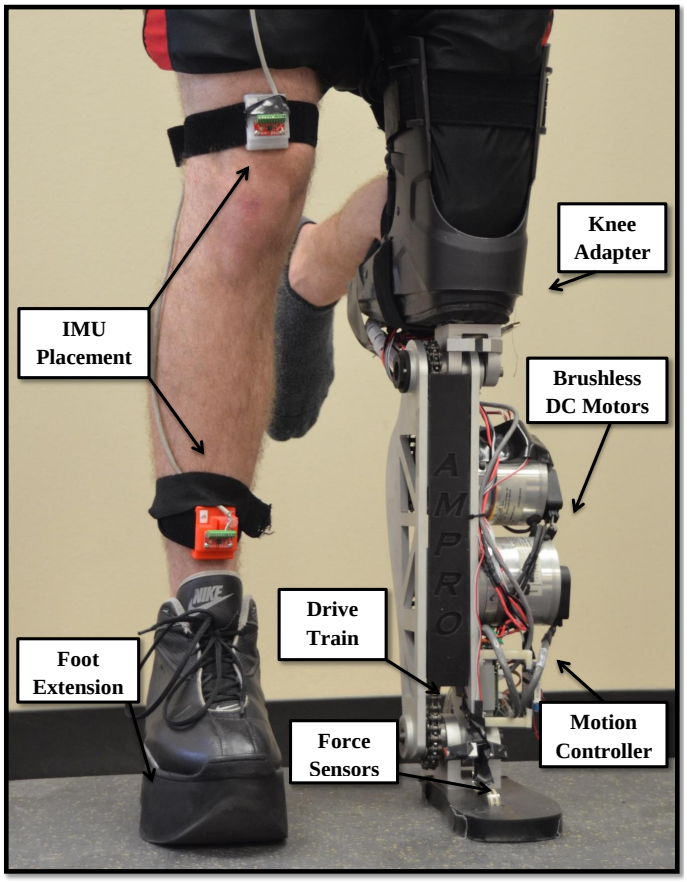

Figure 4.1: Technical diagram of AMPRO I.

The main goal for the design of AMPRO was to produce a very powerful prosthesis with the ability to perform operation modes of an average humans day-to-day life. Motivated by human locomotion and previous works in this area [40, 12], AMPRO I is designed as a self-contained anthropomophic powered prosthesis.

Most of the requirements posed for the first iteration of AMPRO stem from previous research and published findings on the human body [17, 40, 25]. Specifically, for performance requirements, a 75 kg subject uses approximately 200 W peak during walking. Similarly, an appropriate range of motion was determined to be 100° of flexion for the knee; and 45° of planterflexion paired with 20° of dorsiflexion for the ankle by [29]. When designing AMPRO I, power and torque were the central focus. As a result, AMPRO I has limitations with regard to range of movement and weight (see Table 4.1). This has the potential to cause problems with the test subject during operation, and these shortcomings will be discussed later.

4.1.1 Transmission

Fig. 4.2 illustrates the design of AMPRO I's transmission system. The transmission, of any system, is key to pushing performance to the best possible level. For a powered transfemoral prosthesis, the goal is to provide a transmission mechanism that offers high torque capabilities, smoothness (no grinding), no hysteresis, and a small footprint dimensionally and massively.

Historically, linear actuators (hydraulics, ballscrews, and linkages) have been favored in the design of powered lower limb prostheses because they can perform under these conditions. However, another appropriate option is a DC motor-gearbox assembly. The difficulty in this solution is selecting the correct gearbox. There are many gearboxes available commercially, yet many of the available products fall short in this application due to size, weight and permissible torque capabilities.

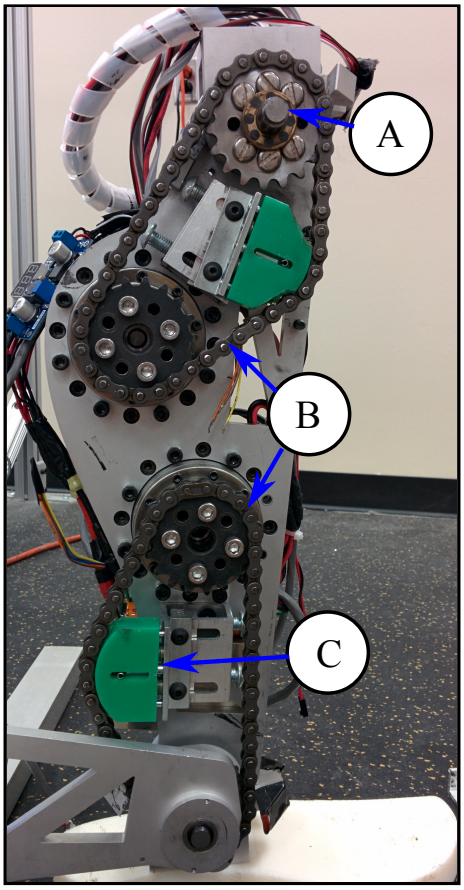

Figure 4.2: Roller chain transmission mechanism of AMPRO I. A shows the knee joint drive shaft. B identifies the location of the output sprocket for both harmonic gearboxes. C illustrates the position of a roller chain tensioner.

In an effort to reduce the overall weight of the device (while also ensuring a self contained end product), a survey of available transmission technologies was conducted to find the best possible design. We concluded (based on available products and their component specifications) that a roller chain connection paired with a harmonic gearbox was the most viable solution to the problem. The harmonic gearbox was selected for its large torque ability, low profile shape and small weight, in spite of its large friction attributes.

Fig. 4.2 shows the technical digram of AMPRO I's transmission. It consists of two of the same transmission assemblies for the knee and ankle joint. A harmonic gearbox is connected to a roller chain sprocket that drives the joint sprocket. The gearbox provides an

80 : 1 ratio while the roller chain delivers a 1 : 1 ratio. At the middle of the roller chain is a tensioning mechanism that uses a lubricative polyethylene plastic. The knee transmission connects to a custom made knee adapter and the ankle transmission connects to a custom made foot.

4.1.2 Motor Selection

Motor selection for the transmission was primarily influenced by the power requirements, torque requirements and weight of the component. After an exhaustive survey of available products, the search was narrowed to 4 potential candidates.

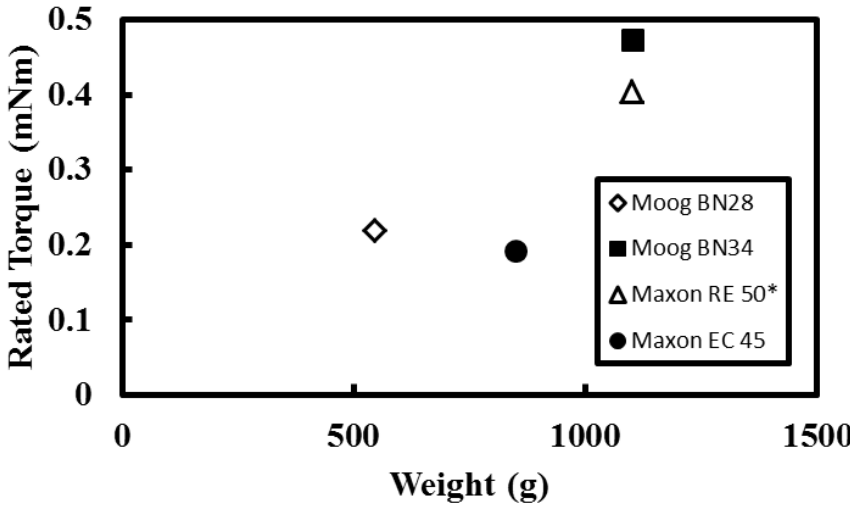

Figure 4.3: Comparison of DC motors.

In the above figure, four potential motors are compared by the rated torque value and weight. Recall that for this device, the goal is to make a prosthesis with enough torque and power to be able to walk on level ground and possibly perform other more difficult tasks.It is for this reason that both the Moog BN34 and Maxon EC 50 stood out from the other motors. It was eventually settled that Moog BN34 motor would be used for its large power

and torque capabilities while still maintaining the same weight as the potential Maxon motor.

4.1.3 Encoder Selection

From the selected transmission and motor, a method of sensing joint angles was required for the device. Since the mechanical advantage of the device is 80, the gain of the encoders will increase. While the ideal solution is to use an encoder at the motor and at the joint, the assumption that minimal compliance was inherent in the system was used. This assumption requires only one encoder located at each motor shaft and reduces the overall cost of the device. Also, a lower encoder resolution could be utilized due to the large mechanical advantage and encoder located at the motor shaft.

An estimated operation space of 0.02 rads would be required for the device to have acceptable performance. Therefore the required resolution of the encoder would be on the order of 4,000 counts per revolution. In the past, such resolutions are not unheard of for use in robotics. It was eventually determined that two incremental encoders would be used for the prosthesis. Optical incremental encoders are traditionally used for high resolution applications where high speeds are present. Incremental encoders were chosen over absolute encoders, again, because of the low profile nature of incremental encoders. However, on issue encountered with this type of encoder is the requirement that the encoder must be calibrated before each trial with the device to avoid drifting.

4.2 Prosthesis Components

AMPRO is designed with a focus on high powered, compact and structurally safe operation. The device utilizes a roller chain drive train for actuation of both knee and ankle joints. This transmission uses a brushless DC motor (Moog BN34) and a harmonic gearbox (model CSG-2UH-LW) for actuation in the sagittal plane. For sensing purposes, two incremental encoders are located at each motor and the device is designed to incorporate

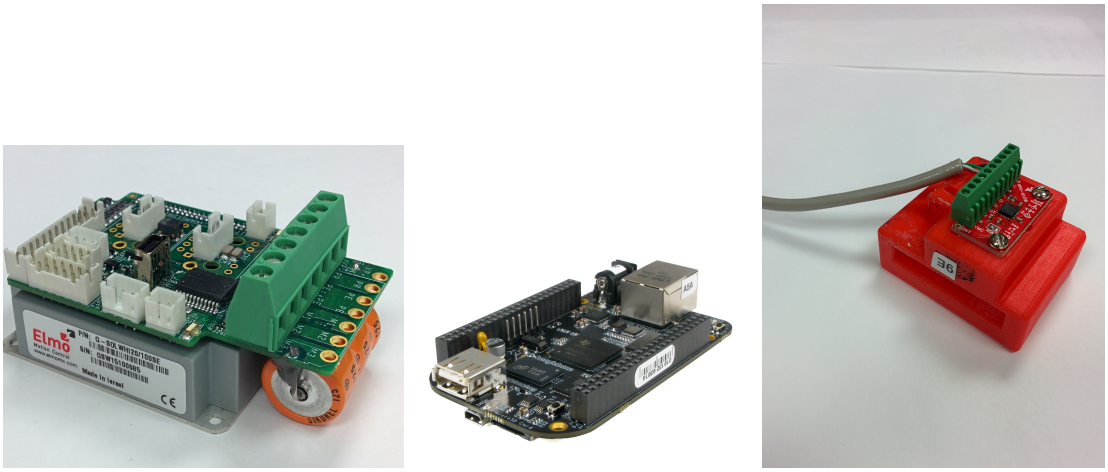

Figure 4.4: Electrical components used on AMPRO I. Elmo Motion Controller (left), BeagleBone Black (center) and Inertial Measurement Unit (right).

absolute encoders at the actuated joints. Additionally, Two Elmo motion controllers are utilized for low level control of the motors. Two FlexiForce (Parallax 30056) sensors are located on the bottom of the foot and are used to measure the normal reaction forces of the prosthesis.

The primary structure consists of two 7075-T6 aluminum plates designed to accommodate an 80 kg subject through all phases of actuation. A finite element analysis was conducted with SolidWorks to verify a factor of safety between 3 and 5.6 depending on operation conditions. Fig. 4.1 depicts the technical specifications of AMPRO. Furthermore, the self-contained prosthesis uses a 29.6 V LiPo battery and two Beaglebone processors connected via crossover cable for control implementation. These items (not visible in the figure) are attached to the subject's waist via a belt.

The foot of the device is custom designed to allow for the use of a standard pyramid connector or direct connection at the ankle joint, thus enabling height adjustments at the ankle. In addition, experiments involving healthy human subjects use a custom made knee locking adapter that also benefits from the options of using a pyramid connector or direct

Table 4.1: AMPRO Specifications

Parameter	Value
Total Weight (Kg)	8.1
Peak Torque (Nm)	170
Peak Power (W)	374
Allowable Dorsiflexion (deg)	20
Allowable Plantar flexion (deg)	30
Allowable Knee Extension (deg)	5
Allowable Knee Flexion (deg)	70
Height (mm)	409
Width (mm)	165
Max Joint Velocity (rpm)	81.25

connection to the knee joint.

4.3 Experiment

The PD based gait control strategy was implemented to track the reconstructed trajectories obtained in Sec. 2.1 on the self-contained device using the knee locking adapter and a healthy human subject. As seen in Fig. 4.1, the knee locking adapter connects directly to AMPRO in-line with the human subject. By way of design, the immobilized leg of the subject is unable to hinder the operation of AMPRO with minimal discomfort in spite of the asymmetry in the coronal plane.

Walking trails were performed on a treadmill providing a constant speed of $0.625\,\mathrm{m/s}$ which allows for increased safety for the human subject (with the use of handrails) and the researchers monitoring experiments. During each experiment, data recorded from the joint sensors and feedback from the human subject were used to tune the controller gains. The iterative direct feedback between the user and sensor data proved to be conducive for obtaining the best performance of the device.

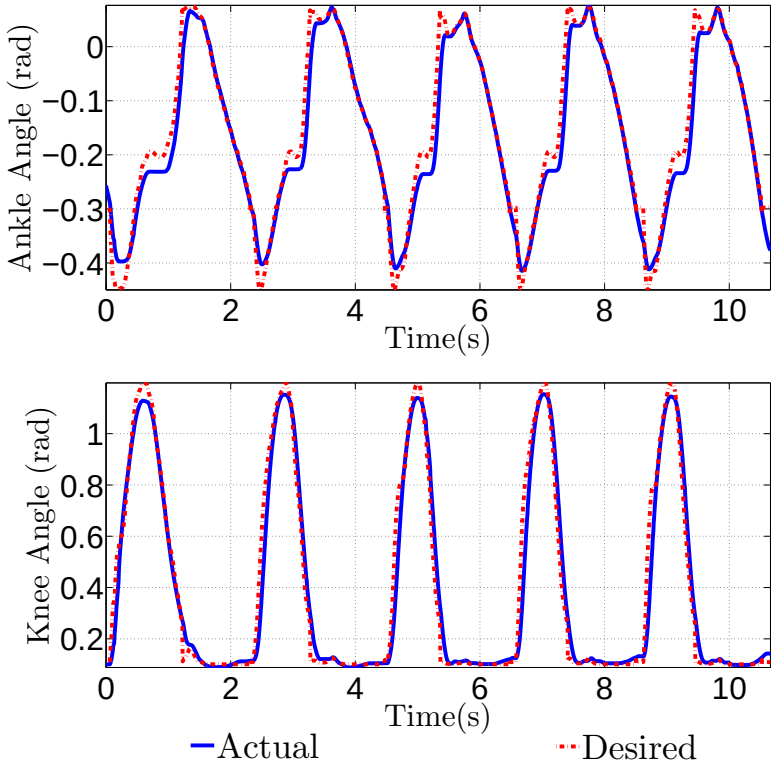

Figure 4.5: Tracking performance for prosthetic joints. Max error = 0.07 with rms error = 0.052 for the ankle joint, and max error = 0.208 with rms error = 0.095 for the knee joint.

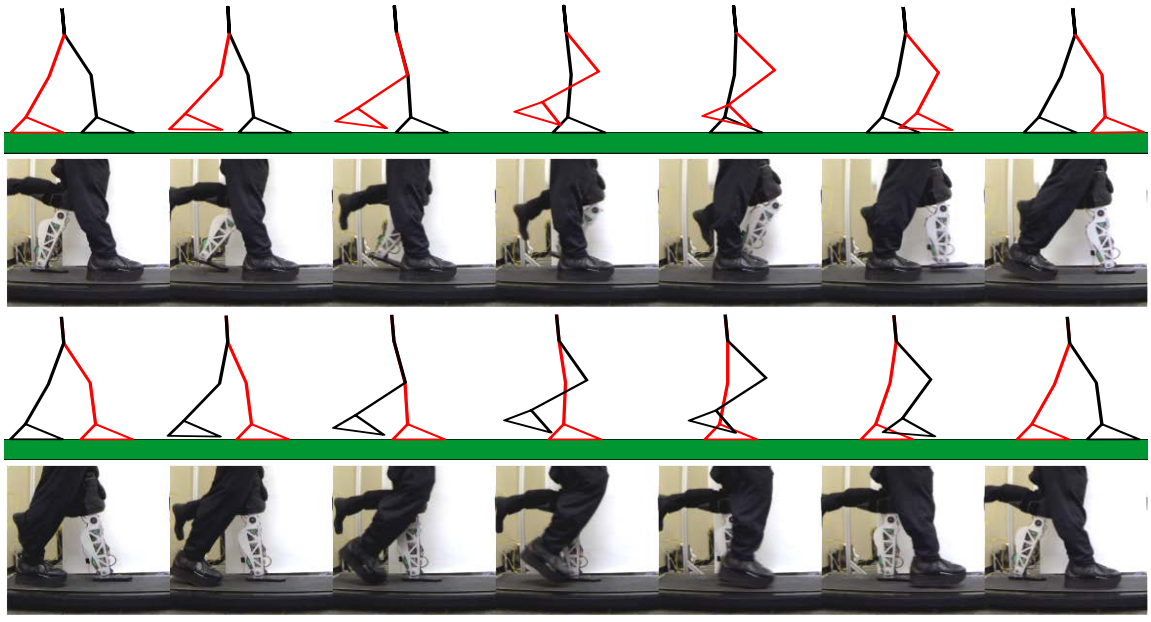

Figure 4.8: Gait tile comparison between the experimental walking and the simulated walking.

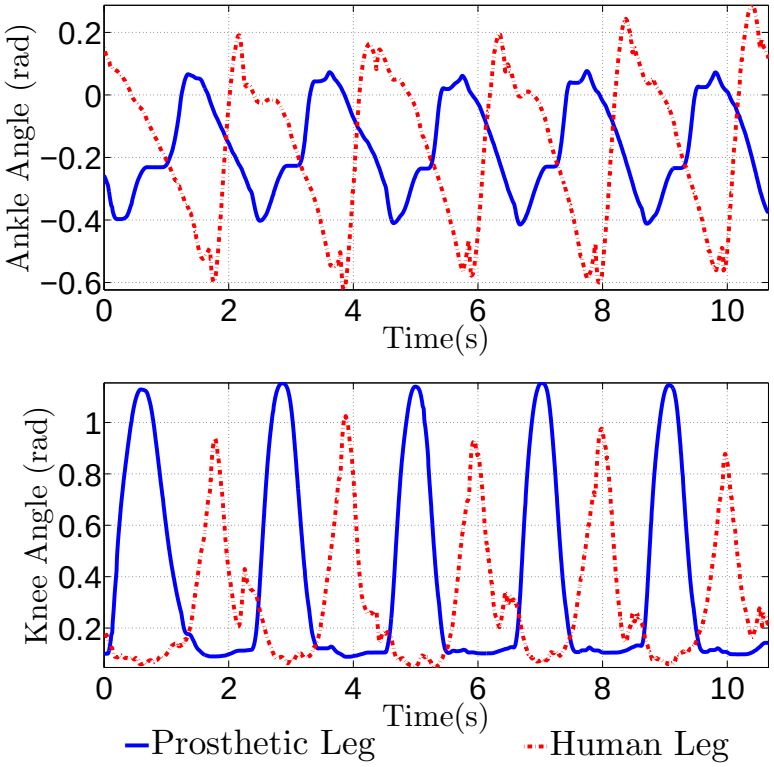

Figure 4.6: Comparison between the heathy and prosthetic joints.

AMPRO has achieved stable human-like walking with a human subject wearing it; the all-encompassing process of obtaining this walking is shown in the video [4]. In particular, from the video, one can notice that AMPRO is robust enough to walk on ramps. For level ground walking, the actual joint angles of multiple steps along with the desired joint trajectories are shown in Fig. 4.5. From this figure, one can verify that AMPRO is able to track optimized human trajectories to within 0.052 and 0.095 (*rads*) RMS error for the ankle and knee joints respectively. Fig. 4.6 illustrates the natural behavior exhibited by AMPRO when compared to the measured human joint angles. In addition, the torques at the ankle and knee joints for five successive steps are shown in Fig. 4.7.

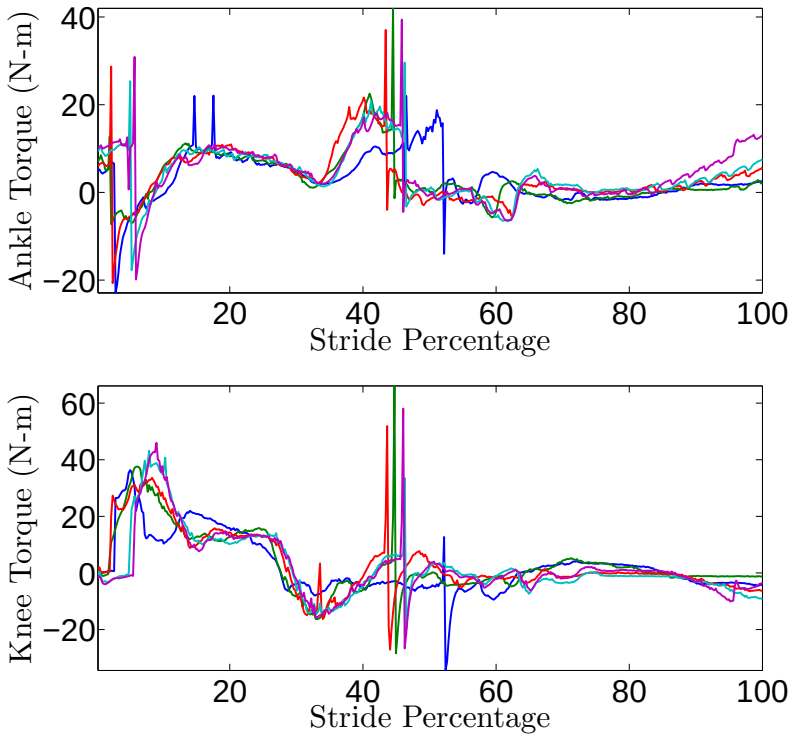

Figure 4.7: Torque supplied by AMPRO to the user for the ankle (top) and knee joint (bottom). The step cycle starts from swing phase.

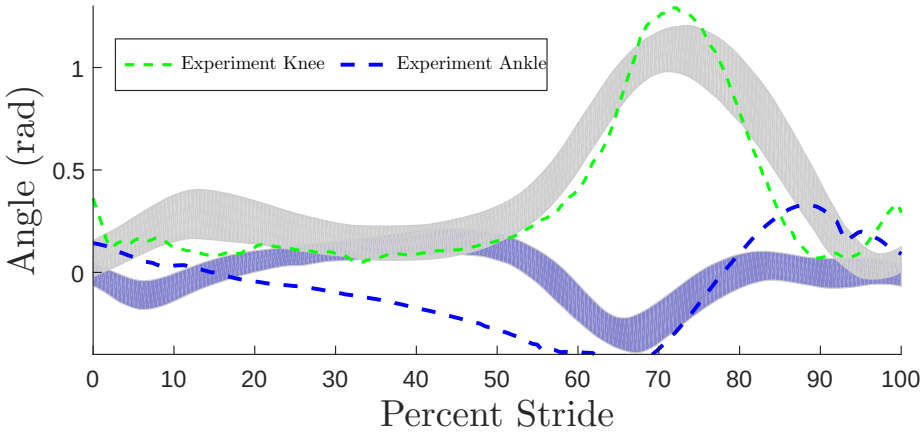

Figure 4.9: IMU measurements during experimentation with AMPRO I compared to nominal trajectories obtained by Winter (Shaded region) [45]

4.4 Results and Conclusions

From the experimental results shown, some interesting findings can be observed. Specifically, one can observe half way through the stride that the switch from swing to stance phase occurs at different times for each step in Fig. 4.7. This phenomena happens because the user progresses through each step at a different pace (from IMU feedback), and AMPRO is able to react accordingly. Additionally, Fig. 4.6 reveals how well AMPRO I restores the walking gait of the test subject. From inspection, one can see that the IMU measurements of the healthy leg closely resemble that of the prosthesis trajectories. However some discrepancies are noticeable, specifically, the the ankle trajectory is much smaller than the actual human measurement. This is best explained by the gait specifically designed for this experiment. As explained previously, a flat-footed walking gait was designed for implementation on AMPRO I. This type of gait will cause a smaller magnitude ankle trajectory and a larger magnitude knee trajectory.

Overall, it was determined that other factors played a significant role in AMPRO I's performance. First, feedback from the test subject brought to light the impact of the weight of AMPRO I. AMPRO I's large weight placed unnecessary strain on the user, and had the potential to significantly impact the performance of the human-prosthesis system. Second, the first iteration of AMPRO failed to account for the height of the user interface for the device. The large size of AMPRO I made operation with the device cumbersome and un pleasant at times. Therefore, a new iteration of AMPRO was conceived to address these possible short comings.

5. DESIGN OF AMPRO II AND CONCLUSIONS

The objective of this section is to introduce the pertinent design specifications of AMPRO II and explain the experiments conducted to obtain human-like locomotion. The design of AMPRO II diverges from AMPRO I by maintaining a focus on weight reduction.

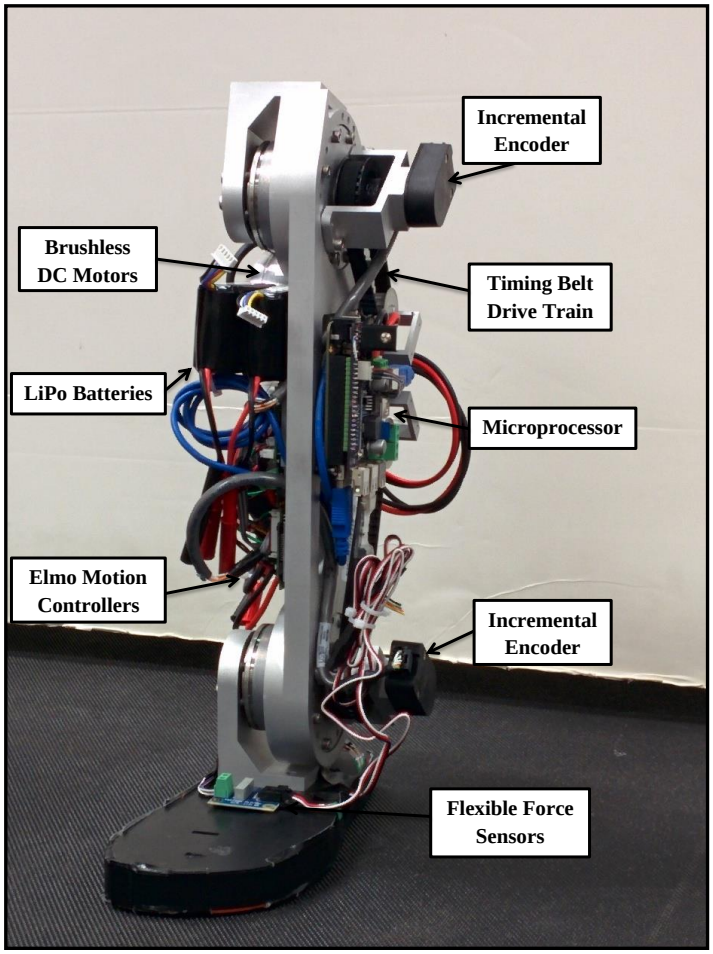

Figure 5.1: Technical diagram of AMPRO II.

5.1 Component Selection

As previously stated, this iteration of AMPRO shifts the center focus to a lightweight design. With this in mind a similar transmission as AMPRO I was used, but with some slight modifications. However some of the same components are used in this device: A harmonic gear box is used at both joints (100 : 1 reduction ratio), a Moog Components Group DC motor is also used for each joint (Model BN-28 silencer series) and the same incremental encoders are used to sense joint angles and angular velocities.

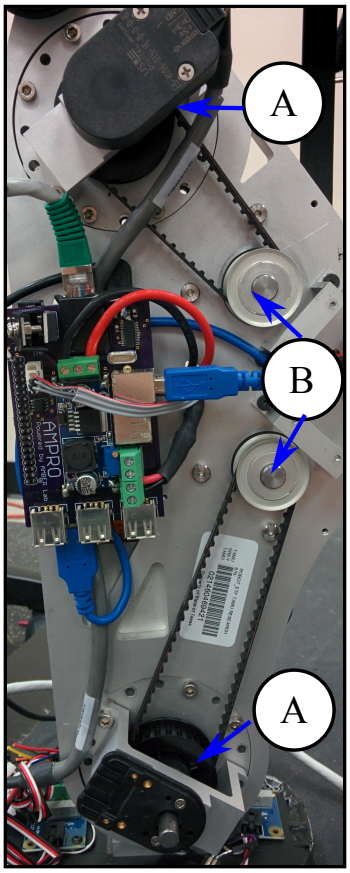

Figure 5.2: Timing belt transmission mechanism of AMPRO II. A notes the location of the input to both harmonic gearboxes. B indicates the location of the driving motor shafts.

Fig. 5.2 pictures the drivetrain of AMPRO II. From the figure one can see that the most dramatic difference is the separation of the gearbox and motor. Both motors are located at the same position as the human calf muscle (approximately upper middle section), while either gearbox is located in line with the knee and ankle joint axis of the device. Another change from the previous design is the usage of a timing belt drive train. This drivetrain is a viable solution only because the gear box and motor are not directly connected. This separation allows for an intermediate pulley reduction between the motor and gearbox. Therefore, rather than the pulley having to endure the output torque of the gearbox, the pulley mechanism must only withstand the torque supplied by the motor which is well within the limitations of the timing belt.

With a lightweight design in mind, we again revisit the four motors considered previously. Fig. 5.3 shows a comparison of four possible motor solutions with an emphasis on weight and size.

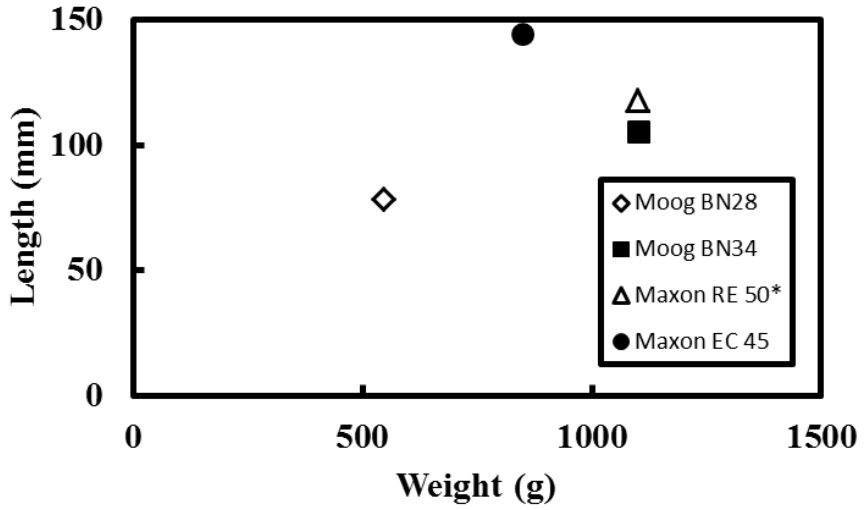

Figure 5.3: Comparison of DC motors.

In the above figure the Moog BN28 DC motor clearly dominates the other possible choices while still providing sufficient torque requirements. Eventhough the new motor

Table 5.1: AMPRO iterations compared to existing prostheses. Values for Vanderbuilt prosthesis obtained from [24]

Parameter	AMPRO I	**AMPRO II**	Vanderbuilt
Total Weight (Kg)	8.1	**4.8**	5
Peak Torque (Nm)	**170**	120	85 to 110
Rated Motor Power (W)	**374**	210	*
Knee Motion Range (deg)	-5 to 70	-5 to 80	**-5 to 115**
Ankle Motion Range (deg)	-40 to 30	**-60 to 60**	-45 to 25
Height (mm)	409	**345**	425
Width (mm)	165	**119**	*
Max Joint Velocity (rpm)	**81.25**	80	*

selected will reduce the continuous torque supplied, results from AMPRO I showed that the device never used its full potential. Additionally, this change in motors allowed for a reduction in the overall weight of the device by 1 kg.

5.2 Experimentation

The PD based gait control strategy was implemented on the self-contained device using the knee locking adapter and a healthy human subject. Walking trails were performed on a treadmill providing a constant speed of $0.625 m/s$, which allowed for increased safety for the human subject (with the use of handrails) and the researchers monitoring experiments. During each experiment, data recorded from the joint sensors and feedback from the human subject were used to tune the controller gains. The iterative direct feedback between the user and sensor data proved to be conducive for obtaining the best performance of the device. Experimental results of the device can be seen in the following figure.

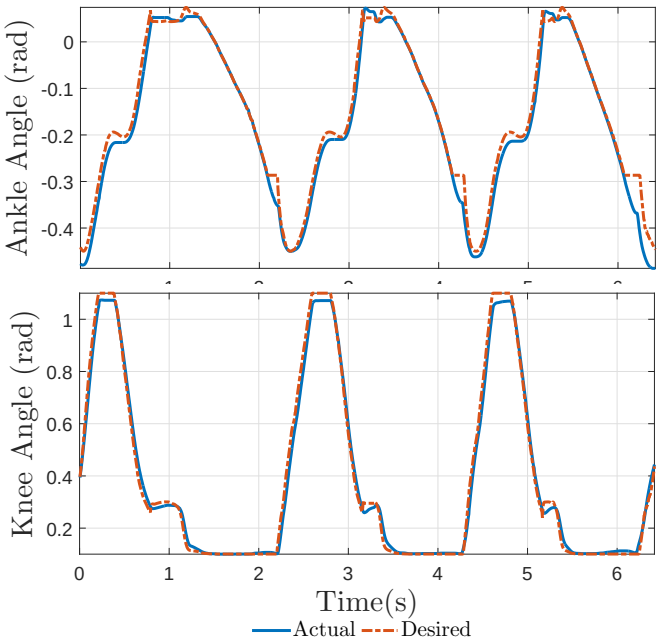

Figure 5.4: Tracking performance for prosthetic joints of AMPRO II. Rms error = 0.033 for the ankle joint, and rms error = 0.074 for the knee joint.

AMPRO II has achieved stable human-like walking with a human subject. For level ground walking, the actual joint angles of multiple steps along with the desired joint trajectories are shown in Fig. 5.4. From this figure, one can verify that AMPRO II is able to track optimized human trajectories to within 0.033 and 0.074 (*rads*) RMS error for the ankle and knee joints respectively. Fig. 5.6 illustrates the natural behavior exhibited by AMPRO when compared to the measured human joint angles. This figure also serves as a basis to visually observe how the prosthetic device closely mirrors the performance of the healthy leg.

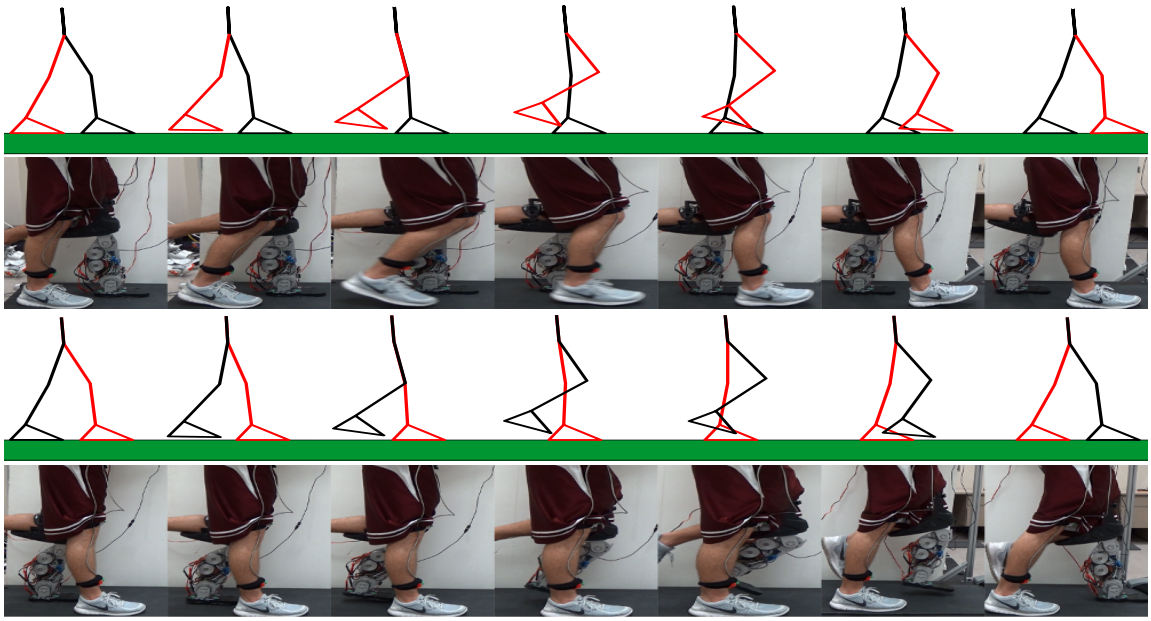

Figure 5.5: Gait tile comparison between the experimental walking and the simulated walking.

In addition, the torques at the ankle and knee joints for five successive steps are shown in Fig. 5.7. One can observe half way through the stride that the switch from swing to stance phase occurs at different times for each step. Also, at the beginning of the step one will see that the same shape is present for each step but occurs at different times. This phenomena happens because the user progresses through each step at a different pace (from IMU feedback), and AMPRO II is able to react accordingly.

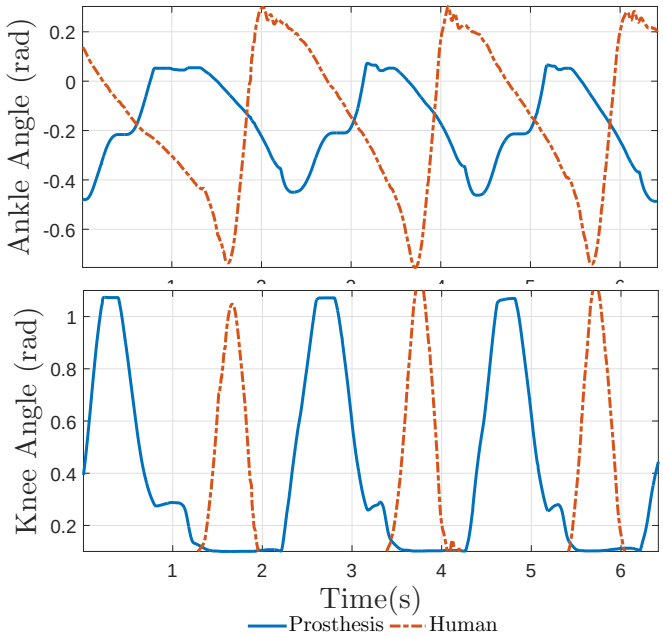

Figure 5.6: Comparison of IMU measurements to AMPRO II joint angles.

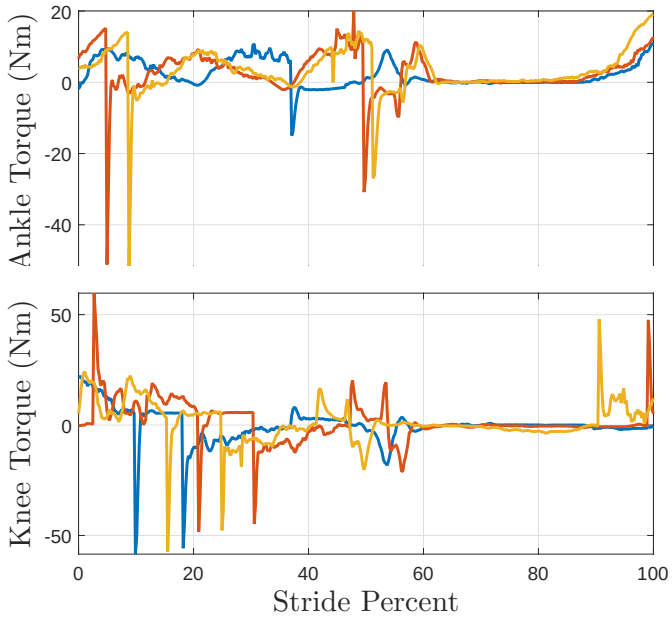

Figure 5.7: Measured torque output of AMPRO II for 3 steps.

5.3 Results and Conclusions

Analysis of the results revealed that AMPRO II actively supplied power to the user during a flat-footed walking experiment. It is of note that the AMPRO II's trajectory during the experimentation has some differences compared to that of a normal leg trajectory (see Fig. 5.6). These phenomena are best explained by recalling the walking behavior and control design used for this research. During operation, AMPRO is programmed to track an optimized flat-footed walking gait, which is not the typical behavior of most human subjects. Similar research can be found in [34]. This drawback will be improved in future work by considering a more natural looking multi-domain walking gait.

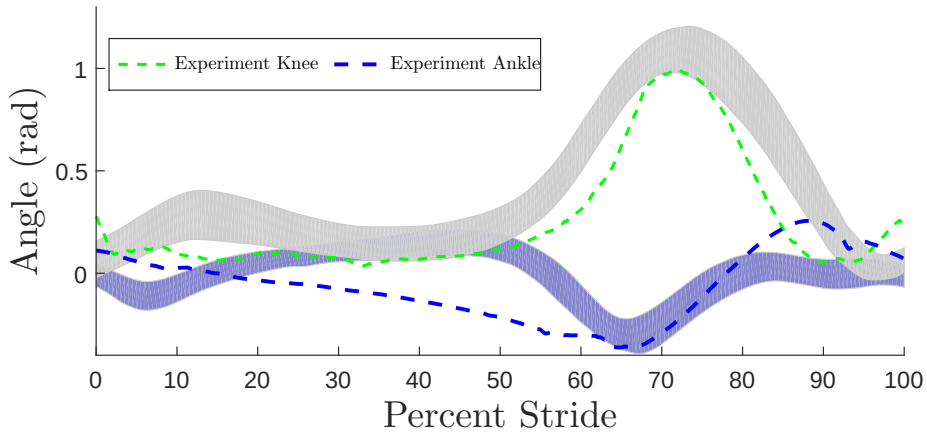

Figure 5.8: IMU measurements during experimentation with AMPRO II compared to nominal trajectories obtained by Winter (Shaded region) [45]

In Fig. 5.8, the average IMU measurements recorded during experimentation are plotted against the nominal values for human walking [45]. From this plot, it is observed that during operation of AMPRO II, the user very closely restores a natural walking gait. However, unlike passive devices, AMPRO II supplies active power to the user during locomotion.

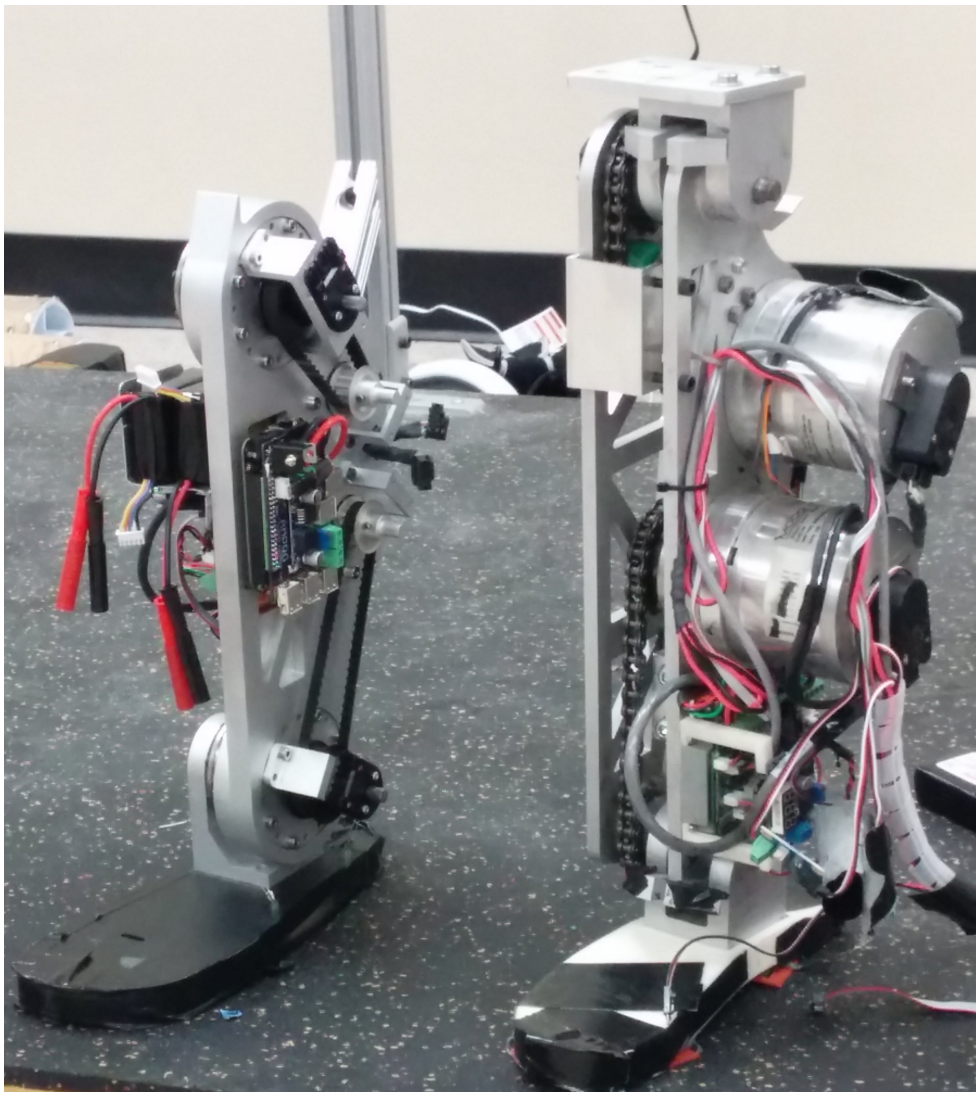

Figure 5.9: Comparison between AMPRO I (right) and AMPRO II (left).

The main objective of the design of AMPRO II, however, was to create a lightweight device with a small form factor to improve the human-prosthesis system performance. From the above discussion, one can see that reducing the weight of the first iteration of AMPRO (through various design changes), allowed for some quantitative improvement in the performance of the system through a reduction in e_{rms}. Additionally, because the weight of AMPRO II very closely replicated that of the test subject's residual limb, the test

subject felt more comfortable operating the device. This inclusion of weight similarity of the test subject could be responsible for the increased restoration of the natural gait for the test subject. However, in light of the the improvements seen from AMPRO I to AMPRO II, much work can still be done to increase the overall performance of the device.

5.4 Future Work

After analyzing the performance of AMPRO the author has planned future actions to take to improve the performance of the device. A substantial increase in performance is expected with continued improvement to AMPRO's control framework [2]. Future experiments should showcase a comparison between the control approach used in this paper, other standard control options, and newly developed promising control strategies [47], [20], [5]. Another topic for future research is achieving more advanced human behaviors with AMPRO. In this research, the focus was applied to flat-foot walking gaits. This type of gait proved to be effective but introduced some slight differences when compared to a typical walking gait. One way to see a dramatic increase in performance is to incorporate Multi-contact walking [48] [28]. Introducing multiple walking gait domains will inherently make the device more human-like and correct some differences between healthy human data and that presented here [3]. This in turn will further advance the functionality and promise of a smart robotic prosthesis.

REFERENCES

[1] Current day robotic prostheses. http://www.mace.manchester.ac.uk.

[2] AMPRO walks with the nonlinear real-time optimization controller. http://youtu.be/NxJ7nMsJ63o.

[3] AMPRO walks with multicontact walking gaits. https://www.youtube.com/watch?v=K6mKYrVYVwE.

[4] Ampro: From robotic walking to prosthesis. http://youtu.be/mZan3v0XaIY.

[5] N. Aghasadeghi, H. Zhao, L. J. Hargrove, A. D. Ames, E. J. Perreault, and T. Bretl. Learning impedance controller parameters for lower-limb prostheses. *IEEE: IROS*, 2013.

[6] A. D. Ames. First steps toward automatically generating bipedal robotic walking from human data. In *Book chapter of Robotic Motion and Control*, volume 422, pages 89–116, 2011.

[7] A .D .Ames, Eric. A .Cousineau, and Matthew J .Powell. Dynamically stable bipedal robotic walking with nao via human-inspired hybrid zero dynamics. In *Hybrid Systems: Computation and Control*, Beijing, 2012.

[8] A. D. Ames, Kevin Galloway, JW Grizzle, and Koushil Sreenath. Rapidly exponentially stabilizing control lyapunov functions and hybrid zero dynamics. 2014.

[9] A. D. Ames, R. Vasudevan, and R. Bajcsy. Human-data based cost of bipedal robotic walking. In *International Conference of Hybrid Systems: Computation and Control*, volume 14, pages 153–162, 2011.

[10] Aaron D Ames. Human-inspired control of bipedal walking robots. *Automatic Control, IEEE Transactions on*, 59(5):1115–1130, 2014.

[11] S. K. Au, P. Dilworth, and H. Herr. An ankle-foot emulation system for the study of human walking biomechanics. In *IEEE Intl. Conf. Robotics and Automation*, pages 2939–2945, Orlando, May 2006.

[12] S.K. Au, P. Bonato, and H. Herr. An emg-position controlled system for an active ankle-foot prosthesis: an initial experimental study. In *Rehabilitation Robotics, 2005. 9th International Conference on*, pages 375–379.

[13] J.A. Blaya and H. Herr. Adaptive control of a variable-impedance ankle-foot orthosis to assist drop-foot gait. *Neural Systems and Rehabilitation Engineering, IEEE Transactions on*, 12(1):24–31, 2004.

[14] T. Dillingham. Limb amputation and limb deficiency: Epidemiology and recent trends in the united states. *Southern Medical Journal*, 2002.

[15] Grimes D.L. *An Active Multi-Mode Above Knee Prosthesis Controller*. PhD thesis, Massachusetts Institute of Technology, 1977.

[16] W.C. Flowers. A man-interactive simulator system for above-knee prosthetics studies. *Department of Mechanical Engineering PhD Thesis, MIT*, 1973.

[17] W.C. Flowers and R.W. Mann. Electrohydraulic knee-torque controller for a prosthesis simulator. *ASME J. of Biomechanical Engineering*, 99(no.4):pp.3–8, 1977.

[18] J. W. Grizzle, C. Chevallereau, A. D. Ames, and R. W. Sinnet. 3D bipedal robotic walking: models, feedback control, and open problems. In *IFAC Symposium on Nonlinear Control Systems*, Bologna, September 2010.

[19] J. Weber H. Herr and S. Au. Powered ankle-foot prosthesis. *Biomechanics of the Lower Limb in Health, Disease and Rehabilitation*, pages pp.72–74, 2007.

[20] month=June H. Zhao and S. Kolathaya and A. D. Ames, booktitle=International Conference on Robotics and Automation (ICRA) 2014. Quadratic programming and impedance control for transfemoral prosthesis.

[21] Y. Hürmüzlü and D. B. Marghitu. Rigid body collions of planar kinematic chains with multiple contact points. *Intl. J. of Robotics Research*, 13(1):82–92, February 1994.

[22] G. K. Klute and B. Hannaford J. Czerniecki. Muscle-like pneumatic actuators for below-knee prostheses. In *Proceedings the Seventh Int. Conf. on New Actuators*, pages 289–292, 2009.

[23] P. A. Kramer. The effect on energy expenditure of walking on gradients or carrying burdens. *AMERICAN JOURNAL OF HUMAN BIOLOGY*, 22(4):497–507, 2010.

[24] B.E. Lawson, J.E. Mitchell, D. Truex, A. Shultz, E. Ledoux, and M. Goldfarb. A robotic leg prosthesis: Design, control and implementation. *IEEE Robotics and Automation Magazine*, 21(4):70–81, 2014.

[25] H. J. Luinge and P. H. Veltink. Measuring orientation of human body segments using miniature gyroscopes and accelerometers. *Medical and Biological Engineering and computing*, 43(2):273–282, 2005.

[26] W. Ma, H. Zhao, S. Kolathayar, and A. D. Ames. Human-inspired walking via unified pd and impedance control. In *submitted to the IEEE International Conference on Robotics and Automation*, 2014.

[27] N. Miller, O. C. Jenkins, M. Kallmann, and M. J. Mataric. Motion capture from inertial sensing for untethered humanoid teleoperation. In *Humanoid Robots, 2004 4th IEEE/RAS International Conference on*, volume 2, pages 547–565. IEEE, 2004.

[28] D. C. Morgenroth and A. D. Segal. The effect of prosthetic foot push-off on mechanical loading associated with knee osteoarthritis in lower extremity amputees. July 2011.

[29] S. Nadeau, B.J. McFadyen, and F. Malouin. Frontal and sagittal plane analyses of the stair climbing task in healthy adults aged over 40 years: What are the challenges compared to level walking? In *Clinical Biomechanics*, page 530, 2003.

[30] M. J. Powell, H. Zhao, and A. D. Ames. Motion primitives for human-inspired bipedal robotic locomotion: Walking and stair climbing. In *Robotics and Automation (ICRA), 2012 IEEE International Conference on*, pages 543–549. IEEE, 2012.

[31] D. Roetenberg, H. Luinge, and P. Slycke. Xsens mvn: full 6dof human motion tracking using miniature inertial sensors. *Xsens Motion Technologies BV, Tech. Rep*, 2009.

[32] J. Rose and J. G. Gamble. *Human Walking*. Lippincott Williams & Wilkins, Philadelphia, December 2005.

[33] S. S. Sastry. *Nonlinear Systems: Analysis, Stability and Control*. Springer, New York, June 1999.

[34] T. Seel, J. Raisch, and T. Schauer. Imu-based joint angle measurement for gait analysis. *Sensors*, 14(4):6891–6909, 2014.

[35] S. Siegler and W. Liu. *Three-Dimensional Analysis of Human Locomotion*, chapter Inverse Dynamics in Human Locomotion, pages 191–209. John Wiley & Sons, New York, 1 edition, 1997.

[36] R. W. Sinnet, M. J. Powell, Shu Jiang, and A. D. Ames. Compass gait revisited: A human data perspective with extensions to three dimensions. In *50th IEEE Conference on Decision and Control and European Control Conference.*, Orlando, December 2011.

[37] R. W. Sinnet, M. J. Powell, R. P. Shah, and A. D. Ames. A human-inspired hybrid control approach to bipedal robotic walking. In *IFAC World Congress*, Milano, August 2011. Preprint available online: `http://http://www1.mengr.tamu.edu/aames/preprint/`.

[38] S Šlajpah, R Kamnik, and M Munih. Kinematics based sensory fusion for wearable motion assessment in human walking. *Computer methods and programs in biomedicine*, 2013.

[39] Douglas G. Smith. The transfemoral amputation level, part 1. *Amputee Coalition of America*, 14(2), 2004.

[40] F. Sup, A. Bohara, and M. Goldfarb. Design and Control of a Powered Transfemoral Prosthesis. *The International journal of robotics research*, 27(2):263–273, February 2008.

[41] F. Sup, H. A. Varol, and M. Goldfarb. Self-contained powered knee and ankle prosthesis: Initial evaluation on a transfemoral amputee. *IEEE International Conference on Rehabilitation Robotics*, pages pp.638–644, 2009.

[42] D. G. Thelen and F. C. Anderson. Using computed muscle control to generate forward dynamic simulations of human walking from experimental data. 39(6):1107 –1115, January 2006.

[43] E. R. Westervelt, J. W. Grizzle, C. Chevallereau, J. H. Choi, and B. Morris. *Feedback Control of Dynamic Bipedal Robot Locomotion*. CRC Press, Boca Raton, June 2007.

[44] E. R. Westervelt, J. W. Grizzle, and D. E. Koditschek. Hybrid zero dynamics of planar biped walkers. *IEEE TAC*, 48(1):42–56, January 2003.

[45] D. A. Winter. *Biomechanics and Motor Control of Human Movement*. Wiley-Interscience, New York, 2 edition, May 1990.

[46] S. Rahmatalla Y. Xiang, J. S. Arora and K. Abdel-Malek. Optimization-based dynamic human walking prediction:one step formulation. 79(667 - 695):291–305, February 2009.

[47] H. Zhao and A. D. Ames. Quadratic program based control of fully-actuated transfemoral prosthesis for flat-ground and up-slope locomotion. In *American Control Conference (ACC), 2014*, pages 4101–4107, June 2014.

[48] H. Zhao, W. L. Ma, M. B. Zeagler, and A. D. Ames. Human-inspired multi-contact locomotion with amber2. In *Cyber-Physical Systems (ICCPS), 2014 ACM/IEEE International Conference on*, pages 199–210, April 2014.

[49] H. Zhao, M. Powell, and A. D. Ames. Human-inspired motion primitives and transitions for bipedal robotic locomotion in diverse terrain. *Optimal Control Applications and Methods*, 2013.